École polytechnique

Von Kármán vortex street

Project report

QUINTELA CASAL, Julio
ROVINA DE ALMEIDA, Gabriel

Palaiseau, France
November 2014

Contents

List of Figures

1 Introduction

The flux around a cylinder may seem one of the simplest examples of fluid mechanics. However, the richness of the physical laws that determine the behaviour of fluids provokes interesting regimes that have attracted the curiosity of researchers for years.

The system we are dealing with has been an example for the development of the Navier-Stokes theory (cf. Stokes Problem, one of the few exact solutions that can be found in fluid mechanics) and the interaction with the cylinder greatly varies in function of the parameter known as the Reynolds number.

For a short spectrum of values, approximately $50 < Re < 200$, the incident flow presents an instable behaviour in which the boundary layer detaches from the solid creating what we call the Bénard-Von Kármán Instability. This phenomenon provokes (due to the convective velocity that drives the incident flow towards the cylinder) the creation of the Von Kármán Vortex Street in which the vortices created disperse and evolve. This is one of the most beautiful examples of the complexity of this scientific field.

We find this project an excellent opportunity to better understand such a phenomenon alongside applying the contents of the Numerical Fluid Dynamics course. In order to realise the model, we considered all the methods that have been presented to us during these three months: we have finally chosen a full Navier-Stokes fractional step method, a Finite Element Method and a Vorticity Navier-Stokes scheme. We decided to present as final models only the last two due to technical difficulties in the fractional method (notably due to computational time and complexity of the corrective schemes).

A complete Finite Element Method is simulated in which we can observe the creation and transmission of the instability; in the Vorticity method, the cylinder is not present as we focus into the behaviour of the vortex street itself, which is well accomplished using this method.

2 Modelling

The general model consists of a cylinder of diameter d immersed in a flow for which the velocity away from the cylinder follows the x-direction and evaluates u_∞. For computational sake, the domain is limited to a finite region Ω around the cylinder, and the problem assumes the configuration exhibited in Figure 2.1.

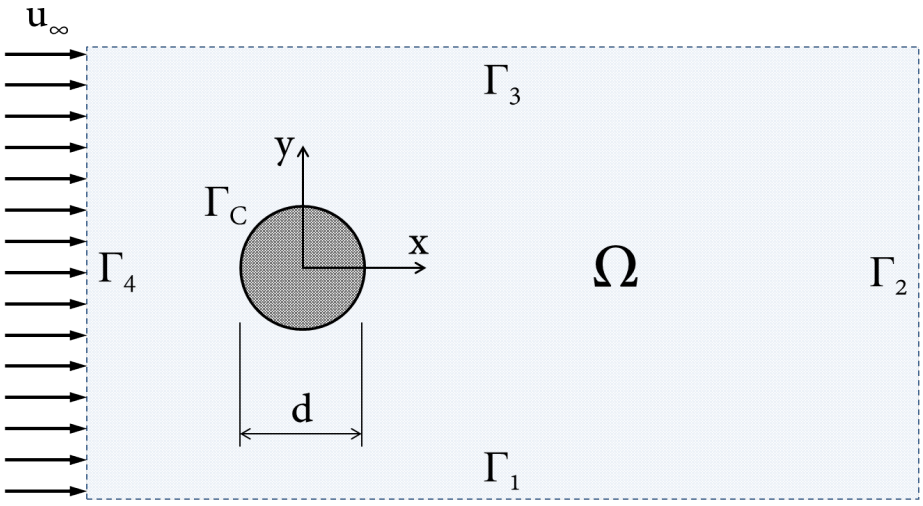

Figure 2.1: Model

We will see later on this report that the studied Bénard-Von Kármán instability is mainly governed by the vortices on the wake of the cylinder. For this reason, only the downstream part of the domain is considered for the vortex analysis.

2.1 Hypothesis

We will work with the incompressible approximation of the Navier-Stokes equations for Newtonian fluids — modelable through a variety of methods —, as we are dealing with low velocities (Mach number much smaller than unity). We shall also suppose that there is no external force applied and that additional frictions in the strain tensor are not applicable.

2.2 Equations

We start therefore from the incompressible Navier-Stokes equations:

$$\rho \frac{D(\mathbf{u})}{Dt} = \mu \nabla^2 \mathbf{u} - \nabla p$$

$$\nabla \cdot \mathbf{u} = 0$$

where $\frac{D}{Dt} := \frac{\partial}{\partial t} + (\mathbf{u} \cdot \nabla)$ represents the material derivative; ρ stands for the density; $\mathbf{u}$, the velocity; μ, the dynamic viscosity and p, the pressure.

Dimensionless form

In order to reduce the number of parameters in the equations and therefore in the analyses, we can define reference values for the studied quantities. Let them be: d for distances, d/u_∞ for time and $\rho\, {u_\infty}^2$ for pressures. By redefining the quantities as a dimensionless prime quantity multiplied by its reference value, the equations can be expressed in a dimensionless form:

$$\frac{D\mathbf{u}'}{Dt} = \frac{1}{Re}\nabla^2\mathbf{u}' - \nabla p' \tag{1}$$

$$\nabla \cdot \mathbf{u}' = 0 \tag{2}$$

This new form of the equations shows that the general evolution of the fluid motion depends on a single parameter, the Reynolds number.

Expected behaviour of the Von Kármán street

Empirically, there are three well studied behaviours in function of the Reynolds number for our system:

For $Re < 1$, we observe a Stokes flow, in which the fluid is perfectly viscous and each streamline is conserved. Convection is thus neglected and an analytical solution is achievable and constitutes an essential part of any undergraduate Fluid Mechanics course.

For $Re > 500$, the system becomes turbulent and thus controlled by complex behaviours that have to be dealt with statistics. The cylinder becomes an 'interference' in the fluid flow and the patterns created show all the complexity of the convective part of the equation, with the consequent modifications of pressure. The Von Kármán vortex phenomena are still observable for a wide range of Reynolds, as the system transitions from a viscosity domination to a pure turbulent regime. The presence of the Von Kármán vortex has been determined to be $47 < Re < 10^5$.

The region between the two systems is a transitional region in which the predominance of factors changes slowly from viscosity to inertia. Bénard and Mallock had established an interval in which the boundary layer gets detached from the cylinder in the posterior part of the cylinder, which creates vortices that oscillate between one side and the other of the body. The frequency has been established empirically by Strouhal in 1878:

$$\frac{fd}{V} = 0.198\left(1 - \frac{19.7}{Re}\right) \tag{3}$$

These vortices get convected by the exterior flow and evolve freely as the rest of the fluid is supposed to be initially velocity free and thus vorticity-free. We finally get what is called the Von Kármán vortex street.

2.3 Boundary Conditions

The boundary conditions that we shall implement in our models are:

- For Γ_4, we shall impose a constant velocity $u_x = u_\infty$ in the horizontal axis, and $u_y = 0$.
- For Γ_1 and Γ_3 we impose $u_x = u_\infty$ and $u_y = 0$ as we consider that the walls are far enough not to be affected by the existence of the cylinder.
- For Γ_2 we impose $p = ct$ and we fix it to 0 in order to avoid growth of the pressure in the model, as pressure acts as a lagrangian multiplicator in assuring $\nabla \cdot u = 0$.
- For Γ_c the boundary condition is adherence, $\mathbf{u} = \mathbf{0}$

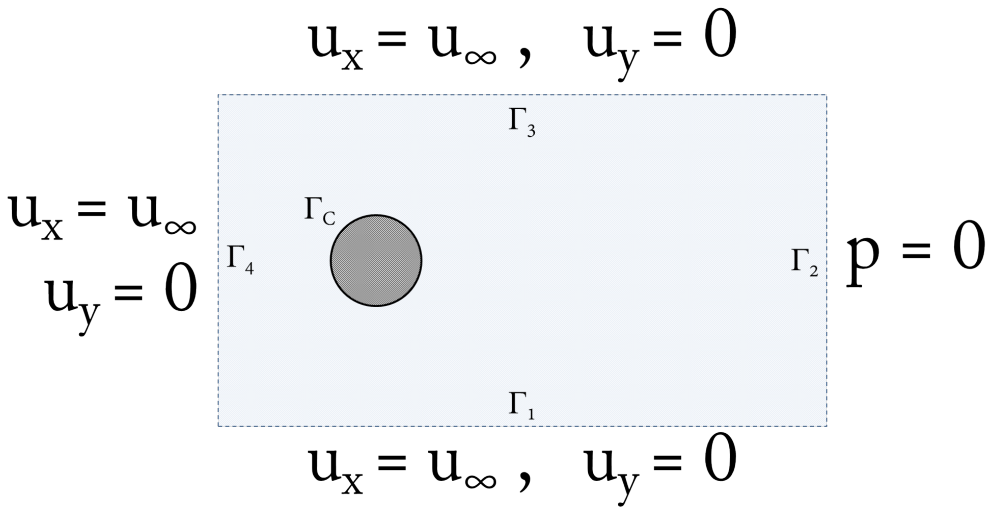

Figure 2.2: Summary of the base conditions

3 Simulation by Finite Element Method

3.1 Modelisation

The method of characteristics

One of the main issues for implementing the Navier-Stokes equations is handling the non-linearity of the advection term. Explicit approaches are generally of easy implementation and enjoy good performance in a general way; the price being poor stability characteristics. Taking this parameter into consideration, we have opted for the method of characteristics. It also offers an explicit treatment of the non-linear term, but presents nevertheless better stability properties than other regular explicit schemes.

This method can be interpreted as the time discretisation for the material derivative of the velocity field. It computes, for a point on the grid, the rate of change in velocity not in relation to the same point, but to the value found on the position where the particle in this point was in the last step, as illustrated in Figure 5.7.

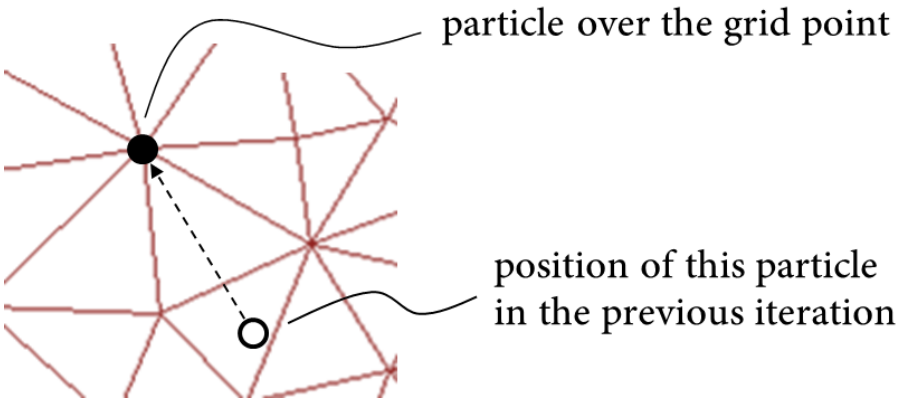

Figure 3.3: Method of characteristics
Backwards integration in time is used to find the previous position of the particle.

For this purpose, this method requires the integration of the velocity field backwards in time, finding in this way the previous position of the advected particle and then its velocity at that moment. Calling X^n an operator that associates the position of a particle on the point x to the position where it was on the previous time step — *estimated with* $\mathbf{u^n}$ —, we can then discretise the material derivative of the velocity in the following way:

$$\frac{D\mathbf{u}'}{Dt'} = \frac{\mathbf{u^n} - \mathbf{u^{n-1}} \circ \mathbf{X^{n-1}}}{\Delta t'} + \mathcal{O}(\Delta t') \tag{4}$$

Note that in order to have an explicit scheme, the operator X is required to perform the backwards integration based on the known velocity field $\mathbf{u^{n-1}}$.

Hence, this approach with the method of characteristics comprises not only a discretisation in time, but also a way around to handle the non-linearity.

Variational formulation

To possibilitate the application of equations 1 and 2 to a Finite Element Method, a variational formulation of the problem should be written. With this finality, we consider two different test functions with compact support over our domain Ω: $\mathbf{v}$, for the velocity and q, for pressure. The equations, discretised with 4, are then multiplied scalarly by their respective test functions and integrated over the domain:

$$\begin{cases} \displaystyle\int_\Omega \left(\frac{\mathbf{u^n} - \mathbf{u^{n-1}} \circ X^{n-1}}{\Delta t'} \cdot \mathbf{v} \right) d\Omega = \int_\Omega \left(\frac{1}{Re} \nabla^2 \mathbf{u^n} \cdot \mathbf{v} - \nabla p^n \cdot \mathbf{v} \right) d\Omega \\ \displaystyle\int_\Omega \nabla \cdot \mathbf{u^n}\, q\, d\Omega = 0 \end{cases}$$

We can then work on these equations integrating by parts, remarking the boundary terms vanish from the fact that we have compact support test functions. The set of equations finally writes:

$$\begin{cases} \displaystyle\int_\Omega \left(\frac{\mathbf{u^n} - \mathbf{u^{n-1}} \circ X^{n-1}}{\Delta t'} \cdot \mathbf{v} \right) d\Omega + \frac{1}{Re} \int_\Omega \nabla \mathbf{u^n} : \nabla \mathbf{v}\, d\Omega - \int_\Omega p^n \nabla \cdot \mathbf{v}\, d\Omega = 0 \\ \displaystyle\int_\Omega q\, \nabla \cdot \mathbf{u^n}\, d\Omega = 0 \end{cases} \tag{5}$$

The equations are complemented with the set of boundary conditions described in 2.3.

3.2 Implementation

The language FreeFem++ was chosen to implement the Finite Element Method for it could simplify steps such as meshing and visualisation of results, allowing us to concentrate on aspects of greater interest to the analysis, namely the boundary conditions and different values of the Reynolds number.

Geometry, meshing, computation

The first step of the implementation consists of defining the geometry of the problem and then meshing the domain. Adjustable parameters for these steps allowed us to concentrate on the necessary aspects of the simulations: a really fine mesh is not necessary far from the cylinder if there is nothing "special" happening there — *e.g.* in the low Reynolds situation; precise calculations and clear visualisation require detailed description of the flow close to the cylinder. This collection of settings allowed us to significantly decrease computational time by adjusting each test to its purposes.

An important detail relies on the choice of the finite elements. As the second equation from 5 imposes constraints to the problem, there must exist a compatible number of degrees of freedom. Consequently, some combinations between the finite elements for the velocity test function and the pressure one may lead to instability problems or statically indeterminate problems. We choose therefore combinations of finite elements that are known to be well posed and convergent, namely P_2 and P_1 or P_1bubble and P_1, for velocity and pressure, respectively.

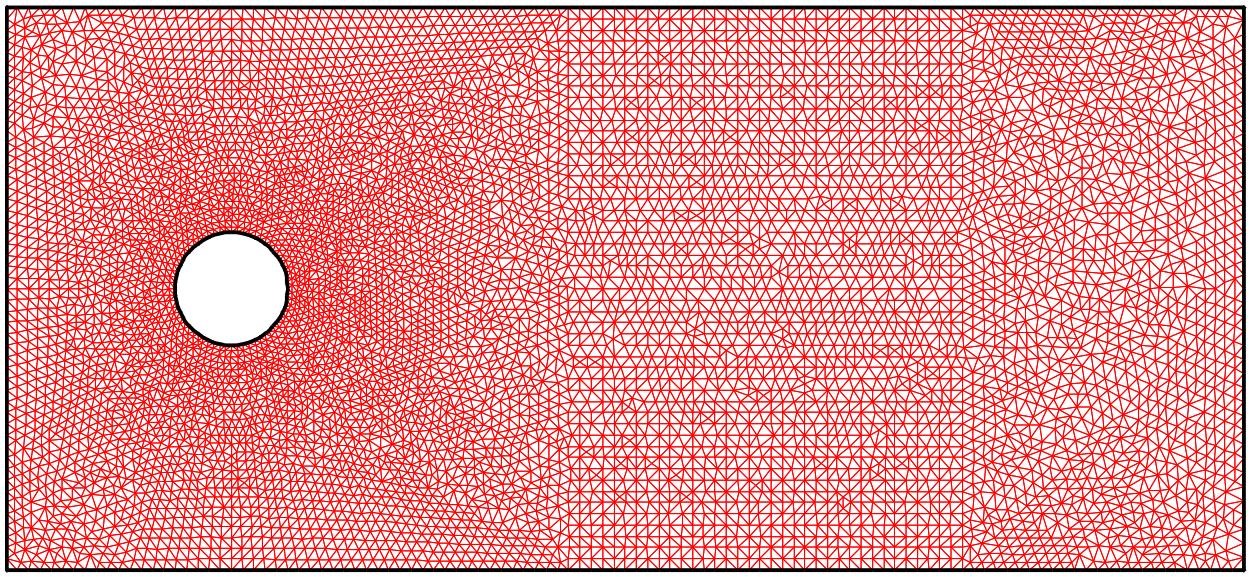

Figure 3.4: Meshing for the Finite Element implementation
Elements are finer closer to the boundary of the cylinder. This is the most detailed mesh used in the simulations and was mainly applied for the generation of images; in the general case, much coarser discretisations were sufficient to provide decent results.

Time marching iterations start with the resolution of the Navier-Stokes problem in its variational form (Equation 5). Then, the velocity field is stored for the next iteration and the algorithm can proceed. For each step, we can analyse and plot quantities such as the vorticity, speed and pressure.

Results are presented in section 5.

4 Simulation by Vorticity Navier Stokes Modelling

4.1 Modelisation

As the main complexities of our system are the oscillating vortex created by the interaction of the fluid's viscosity with the cylinder, a vorticity model is a good choice in order to simulate the behaviour of the vortex street. We chose to create a model using the method of Vortex-in-cell[1]. This code takes advantage of both Eulerian and Lagrangian formulations in order to optimally compute the different components of the Navier-Stokes equations.

Our model constitutes a simplified model of the interaction of the fluid with the cylinder. As we know the behaviour of the system from previous experiences, we know that two vortex are created alternatively in the upper and lower part of the cylinder. Modelling the cylinder in a vorticity mixed scheme can be time consuming and not very interesting: we shall focus in the phenomenological approach to the problem, dealing with the behaviour of two oscillating vortex, representing the upper and lower part of the cylinder. The behaviour shall reproduce efficiently the vortex street as we know it, if our hypotheses are correct.

4.2 Implementation

As advection is best dealt with in a Lagrangian scheme, thus a particular treatment of the field, the diffusive part is most efficient when computed in an Eulerian grid. The hybrid approach used implies a double interpolation: we use particles for the vorticity advection and we interpolate them into the grid in order to diffuse them (thus solving a Poisson equation for the stream function).

The full scheme loop as it has been built in our code is the following:

1. Project and interpolate the particles into the grid
2. Solve the Vorticity diffusion equation on the grid
3. Determine the induced velocity components from the vorticity via a Poisson equation
4. Extract velocities from the stream function and apply them to particles via a grid to particle double interpolation
5. Advect the particles according to their particle-based positions and velocities
6. Eliminate particles that leave the domain by an iteration through all the elements
7. Seed new particles and apply new vortex into the system

8. (optional) Plot the positions of the particles (this may require an additional interpolation of the system)

9. Return to step 1

The boundary conditions have been chosen according to the definitions given above. However, by eliminating the particles that leave the domain we avoid them reaching the conditions in which boundary conditions should be applied so the system is equivalent to having a free boundary, except for the diffusive part in which pressure and vorticity are adjusted to be left free in Γ_2.

5 Results

5.1 Finite Element Method

Simulations have been performed for different values of the Reynolds number. The vorticity isovalues plot provides clear visualisation of the state of the system. Some of the test cases are exhibited in Figure 5.8. It is possible to distinguish three behaviours, confirming the expectations for the flow evolution.

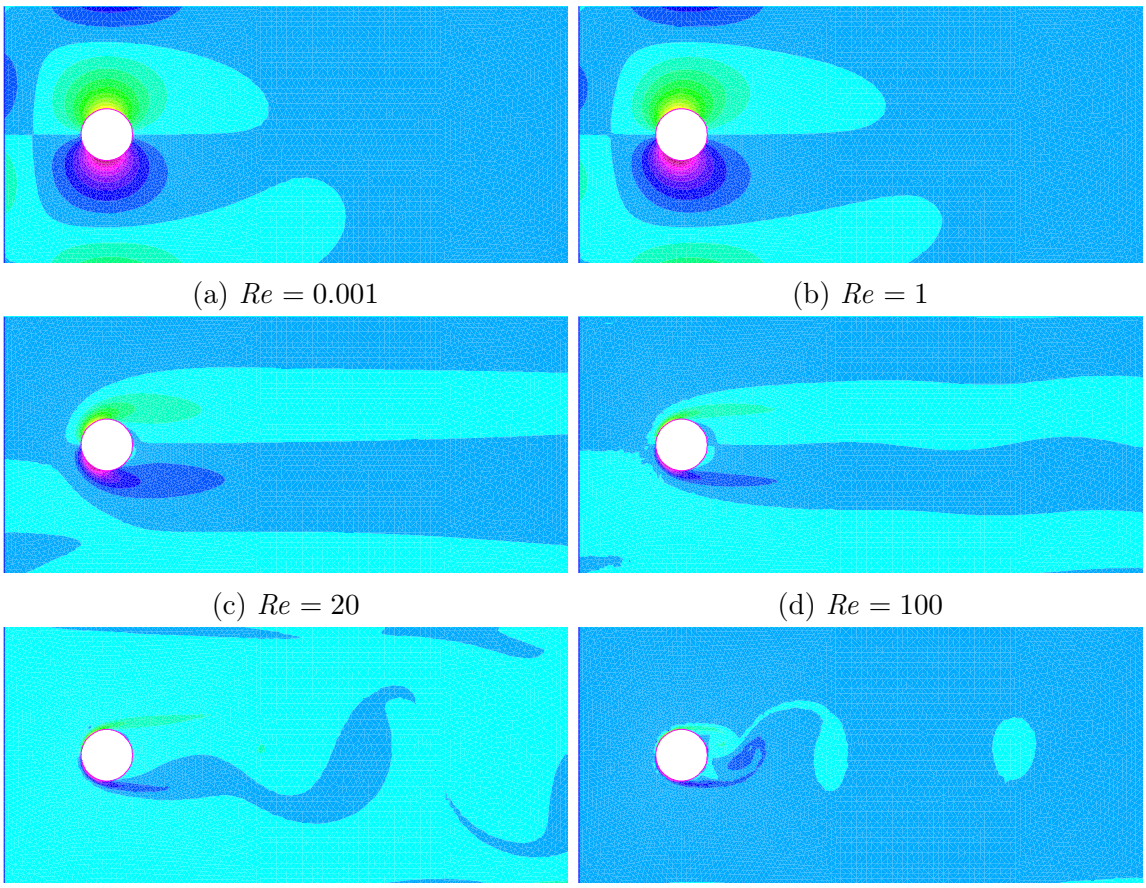

(a) $Re = 0.001$ (b) $Re = 1$

(c) $Re = 20$ (d) $Re = 100$

(e) $Re = 200$ (f) $Re = 500$

Figure 5.5: Flow behaviour for different Reynolds numbers
Images generated at dimensionless time $t = 30$.

At the first Figure (5.9a), corresponding to a very low Reynolds, we can observe that the vorticity on the neighbourhood of the cylinder is practically symmetrical in relation to the vertical diameter. Indeed, the solution behaves similarly to a Stokes flow, *i.e.* the limit when $Re \to 0$.

From the first figure to the second one, we notice very little changes, the remarkable difference being the broken vertical symmetry. If we look at the third one, however, a significant change happens in what concerns the wake behind the cylinder: whereas it was

limited to a small region for the two previous situations, it lasts now for long distances, much greater than the diameter of the cylinder.

Things start to get more interesting at $Re = 100$ (Figure 5.9d): the fluid is similar to the one for $Re = 20$, but for the fact that oscillations start to appear on the wake. This behaviour characterises a transitional state.

Indeed, if we proceed to Figure 5.9e, oscillations increase and the Von Kármán vortices take centre stage: the flow becomes turbulent. This behaviour is mainly controlled by the couple of vortices generated next to the cylinder's surface; they alternate their predominance on the wake flow and the Von Kármán vortex street appears as a consequence. For this very reason, we show in the next section (5.2) that only by modelling these vortices and alternating their strength in the right frequency, we manage to reproduce a vortex street just like Von Kármán's.

A side analysis was performed in order to study the oscillation of the vortices' strengths. Figure 5.6a show the evolution in time of the vorticity for a position close to the upper point of the cylinder. We can also in this analysis recognise the different behaviours we have seen in the previous images. The bottom vortices have analogous curves but the oscillation is dephased of $\pi/2$ (Figure 5.6b).

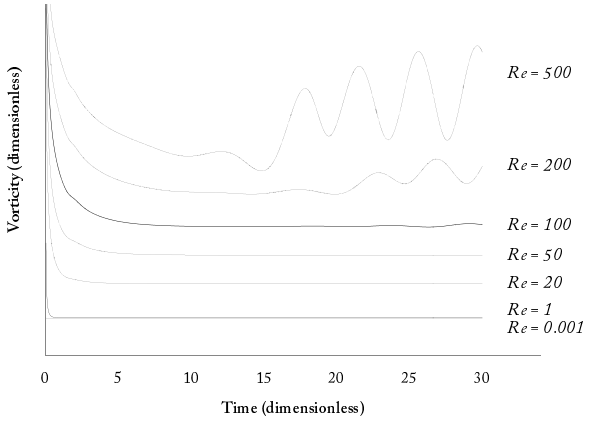

(a) Vorticity above the cylinder

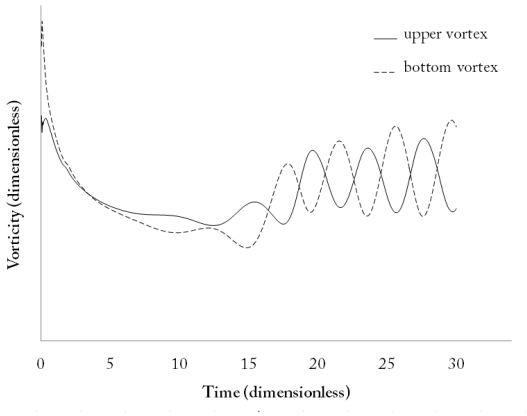

(b) Comparison of vortices

Finally, if we increase the Reynolds a bit further, the vortex street loses its continuous character and starts to emit discretised vortex blobs. At this point, the analysis fulfils the aims of this project and further increments of Re are left for the most curious readers to try at home.

5.2 Vorticity Model

In order to verify the potential of the model to fulfil our needs, we tried to adapt the numerical factors to produce an acceptable visual result. In effect, our results reproduce perfectly the

behaviour of the vortex street, as we can see in the following figure:

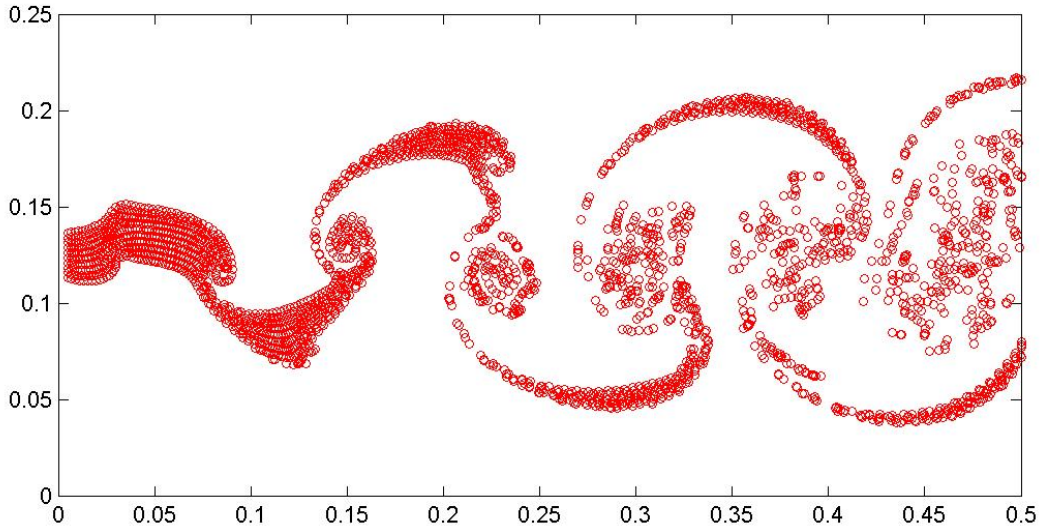

Figure 5.7: Example of result using the Vortex-in-cell model to simulate Von Kármán streets

In this system we have many adaptable parameters. In order to adapt the problem by auto-similarity, we shall determine the characteristic length L and the characteristic velocity V, as these are related to the Reynolds number and only one variable can be left that is for our system $1/Re = \frac{\mu}{VL}$, where μ is the dynamic viscosity of the fluid. There are two other modifiable parameters: the intensity of the vortex G and the frequency of oscillation from up to down ν. In order to search for similarities between the two studied models, we chose to determine the length of the cylinder $L = 1$ and the characteristic velocity $V = 1$. This leaves us with three variables to adapt.

We choose as Reynolds the highest boundary value, in order to accelerate the phenomenon as much as possible: we have already artificially created the instability so a high viscosity is no longer necessary. Concerning the frequency, using the formula mentioned above by Strouhal, we get for a $Re \sim 500$ a value of $\nu = 0.19s^{-1}$ (our choice is determined by the fact that the equation holds true for $Re > 500$). This implies a vortex alternance at each $1/\nu$, approximately each 5 dimensionless time units T (that we shall consider seconds). We should finally adapt the intensity of our vortices G: as there is no suitable way to do it (other than comparing it with our other FEM system, which we will use for verification) we shall simulate many values and choose the value of G that best represents the Von Kármán vortex street. We first executed a range of 1 to 10. We got the results shown next page.

We refined then our simulation to values between 4 and 7 in order to choose the best possible result.

The final result of our vorticity model is an empirical choice of the G model that suits best the Von Kármán street, the only variable left after adapting to the physical reality all the other parameters. We thus get a full model that reproduces the behaviour of the instability. A different choice of Reynolds number would demand adjusting the period of oscillation and a consequent modification of G, this would be an interesting topic in order to go deeper in the study of this instability.

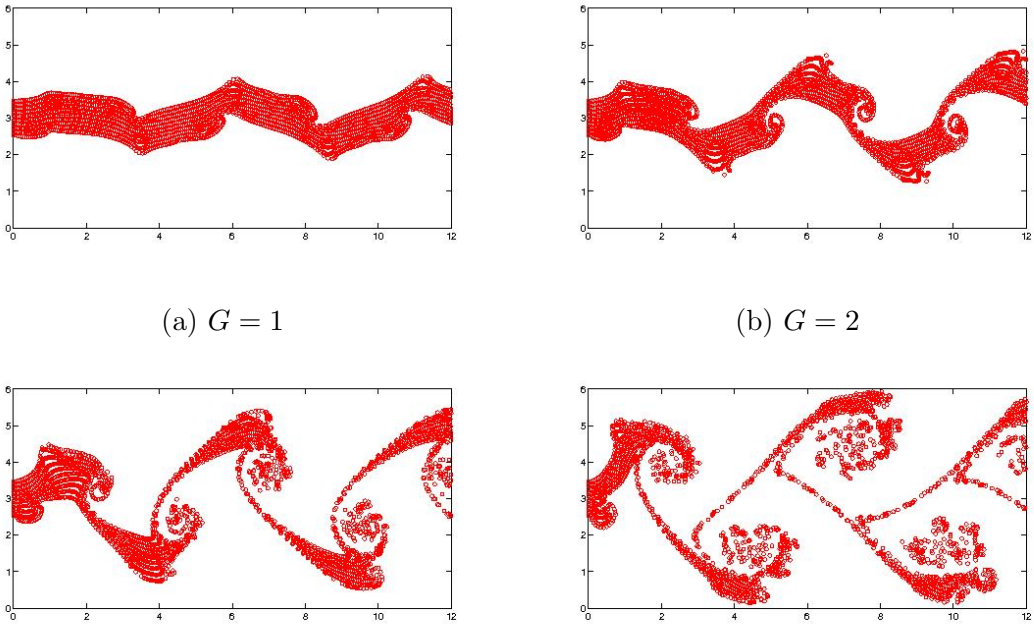

(a) $G = 1$ (b) $G = 2$

(c) $G = 5$ (d) $G = 7$

Figure 5.8: Flow behaviour for different G intensities
Images generated at dimensionless time $t = 50$.

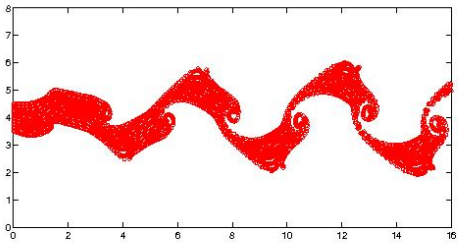

(a) $G = 2.25$

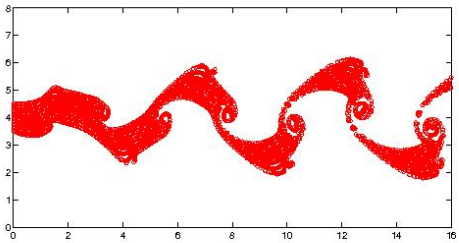

(b) $G = 2.5$

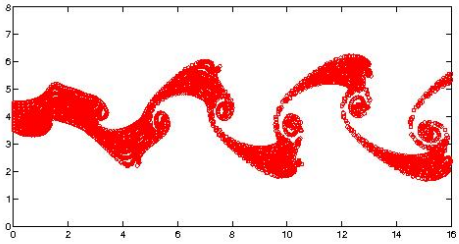

(c) $G = 2.75$

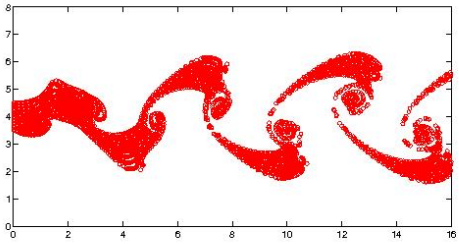

(d) $G = 3$

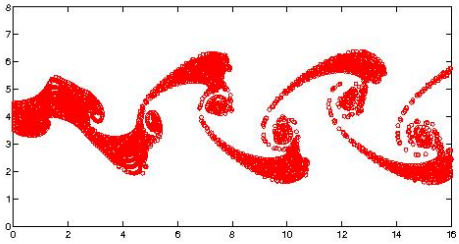

(e) $G = 3.25$

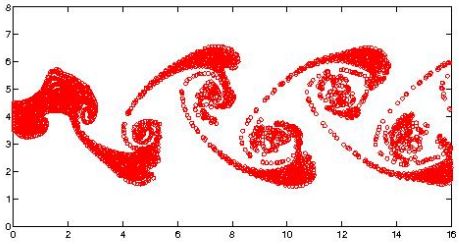

(f) $G = 4$

Figure 5.9: Zoom on the best corresponding Von Kármán street for different G numbers
Images generated at dimensionless time $t = 30$.

6 Conclusion

The two chosen methods have well proven their capability to reproduce the Von Kármán vortex street. The Finite Element Method is especially efficient in processing complex geometries and the model created responds very well to the viscosity interaction with the cylinder, as the mesh had been densified in the proximity of the body. The results reflect the reality of the instability in behaviour, oscillation frequency and shape.

Concerning the Vortex-in-cell model, the code is really efficient and results are clear although the system was quite harder to manipulate as the double interpolations made from particle to grid and back in order to take advantage of the characteristics of the different schemes add complexity to the process. The two codes exhibit a good auto-similarity, which contributes to the validation of the model.

The authors feel pretty satisfied of the final results and consider that it was a really interesting project. The opportunity to model a well-known fluid mechanics paradigm that is not still perfectly understood nowadays has been as enriching as it has been useful to put in practice our knowledge in Numerical Methods for Fluid Dynamics.

References

[1] B. COUET, O. BUNEMAN: Simulation of three-dimensional incompressible flows with a vortex-in-cell method, J. Comp. Phys, 39-2 (1981).

[2] LE TALLEC P.: Modélisation et calcul des milieux continus, Éditions de l'École polytechnique, 2013.

[3] Alouges F., Maury B., *Variational Methods for Computation Fluid Dynamics* - Lecture notes.